ChemComm

COMMUNICATION

View Article Online
View Journal | View Issue

Cite this: *Chem. Commun.*, 2025, **61**, 3367

Received 21st November 2024,
Accepted 17th January 2025

DOI: 10.1039/d4cc06182a

rsc.li/chemcomm

Ionic gradients in flow to control transport of emissive ions†

Lucy L. Fillbrook, ‡[a] Isis A. Middleton, ‡[a] Hamid Rashidnejad, [a] Aditya Sapre,[b] Timothy W. Schmidt, [a] Ayusman Sen [b] and Jonathon E. Beves *[a]

Concentration gradients of simple salts in microfluidic channels control the transport of a common photoredox catalyst.

Controlling how species move in response to chemical stimuli is key for understanding complex biological systems. Microfluidics experiments have provided significant insight into how biologically relevant species spatially respond to changes in their chemical environment, including for nucleic acids,[1,2] proteins,[3] and bacteria.[4] Flow experiments have also been used to monitor the movement of small ionic molecules in response to salt gradients.[5] Suspended particles can respond to salt gradients,[6–9] such as the movement of charged colloids[10,11] in solutions of chloride salts. Salt gradients can also direct and aggregate surfactant vesicles,[12] as well as controlling the formation and movement of DNA and protein-based condensates.[13] Magnetic fields have been used to precisely control the movement of microparticles,[14] and supramolecular nanomotors have been developed with temperature-controlled speeds.[15] Chemotactic studies using host–guest interactions[16,17] or catalysis[18,19] have manipulated macromolecules,[20,21] while other aspects of small molecule diffusion during chemical reactions remain controversial.[22] Despite these examples, control of small molecule movement remains a significant challenge.

Herein we report a simple microfluidics system using the variable diffusivities of ions in sodium salts to generate liquid junction potentials and control the movement of a small cationic dye. We used a microfluidic device with three-inlets (Fig. 1a), based on an established design used for chemotaxis studies.[23] The known diffusivities[24] of Na^+ (1.33×10^{-9} m^2 s^{-1}), Cl^- (2.03×10^{-9} m^2 s^{-1}), and SO_4^{2-} (1.07×10^{-9} m^2 s^{-1}) cause the cation and anion to disperse at different rates and can create a liquid junction potential (Fig. 1b and c). Such liquid junction potentials can be used to control the migration of charged species.

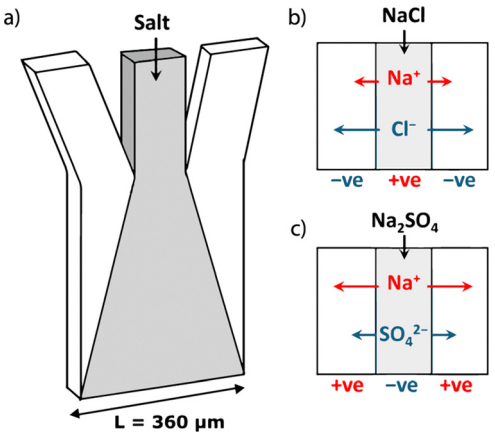

Fig. 1 Schematic representation of salt diffusion down a three-inlet microfluidic device. (a) Three-inlet microfluidic channel, width 360 μm and depth 50 μm. Schematic of ion diffusivities with arrow size indicating relative rate for (b) NaCl and (c) Na_2SO_4.

We first modelled the diffusion of ions when sodium chloride or sodium sulfate are added to the central inlet of a device, assuming the movement of each ion follows a simple Fickian diffusion profile.[17] A full description of the model is provided in ESI,† S3. Fig. 2a shows a simulation of the diffusion of the ions across the channel where the salt is added to the central inlet. Each ion carries a charge, and the different concentration profiles of the cation and anion (Fig. 2b) result in a net charge difference across the channel. At the initial time points the net charge distribution is localised to the boundaries of the channel centre. For sodium chloride, the chloride ions diffuse slightly faster than the sodium ions, generating an area of negative charge just outside the flow of the salt. For sodium sulfate the opposite effect is observed as the sulfate ions diffuse more slowly than sodium ions. At the later time points, the ions

[a] *School of Chemistry, UNSW, Sydney, NSW 2052, Australia. E-mail: j.beves@unsw.edu.au*
[b] *Departments of Chemical Engineering and Chemistry, The Pennsylvania State University, University Park, Pennsylvania 16802, USA*

† Electronic supplementary information (ESI) available: Experimental details and additional data are supplied. See DOI: https://doi.org/10.1039/d4cc06182a

‡ These authors contributed equally.

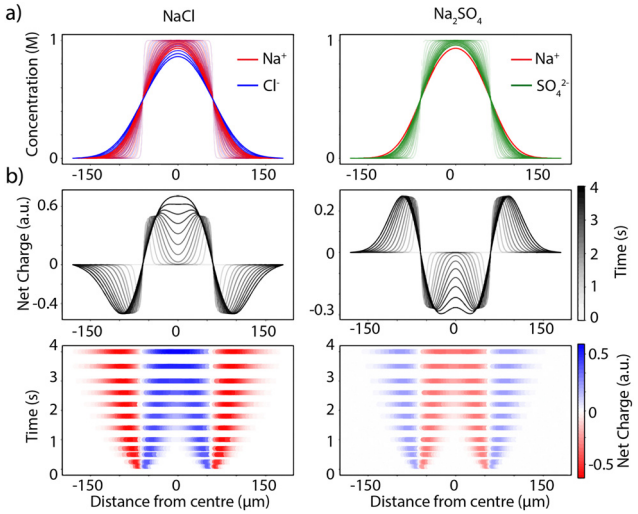

Fig. 2 Modelling the formation of liquid junction potentials based on Fickian diffusion of salt ions over time. (a) The concentration profiles of ions of sodium chloride (left) or sodium sulfate (right) following simple Fickian diffusion after addition *via* the central inlet of a 3-inlet device. (b) The net charge distribution formed across the width of the channel over time as a result of the different diffusivities of the ions shown as a function of charge (middle) or time (bottom).

have diffused further across the channel, and a liquid junction potential is formed. With the sodium chloride salt a net positive charge is formed in the centre of the channel, and with sodium sulfate a net negative charge is formed. This effect is shown in Fig. 2b for comparison with the experimental data.

With this data in hand, we set to monitor the formation of such liquid junction potentials experimentally. We aimed to use optical microscopy with a luminescent dye to measure concentration changes. We selected $[Ru(bpy)_3]Cl_2$ as a small, water-soluble dye which does not readily aggregate in dilute solution and has well-defined photophysical properties.[25] Critically, the visible absorption and emission of this complex are due to MLCT transitions that are only weakly influenced by the ionic strength of the solution. Static absorbance and emission measurements of $[Ru(bpy)_3]Cl_2$ (50 μM) in 2-(*N*-morpholino)-ethanesulfonic acid buffer (MES, 50 mM, pH 6) in the absence and presence of salt (1 M NaCl or 1 M Na_2SO_4), confirmed the emission of $[Ru(bpy)_3]Cl_2$ is a reliable measure of the concentration of the complex under this range of conditions (see ESI,† S4).

We used polydimethylsiloxane (PDMS) based microfluidics devices, mounted on 1 mm glass slides to enable optical monitoring with a high-sensitivity laser scanning confocal microscope. The channel width of the device is 360 μm, depth is 50 μm and length is 4 cm, corresponding to a cross-section of 18 000 μm^2. The emission intensity was measured across the channel width, always at 2 mm from the channel entry point to ensure a stable concentration gradient. Flow rates were varied from 1–20 μL min^{-1} to give residence times in the channel before detection of 0.11–2.16 s. Solutions were flowed through the devices *via* all three inlets simultaneously with identical flow rates. In all cases the emission intensity was normalised across the width of the channel for each time point (see ESI,† S5).

Solutions of $[Ru(bpy)_3]Cl_2$ (50 μM) in MES buffer (50 mM, pH 6) were flowed through all three inlets at variable rates (1–20 μL min^{-1}). The salt was added to the dye stock solution and flowed either through only the central inlet, or through the two external inlets. The experimental data is shown in Fig. 3. Where sodium chloride was added to the central inlet the dye was displaced from the centre of the channel towards the edges (Fig. 3a). Where sodium sulfate was added to the central channel, the dye concentrated in the centre, moving in from the edges (Fig. 3b). These observations match the expected behaviour shown in Fig. 2. The opposite effect was observed when flowing the salt solutions through the two outer inlets rather than the central inlet. That is, where sodium chloride was added to the outer inlets the emission intensity increases

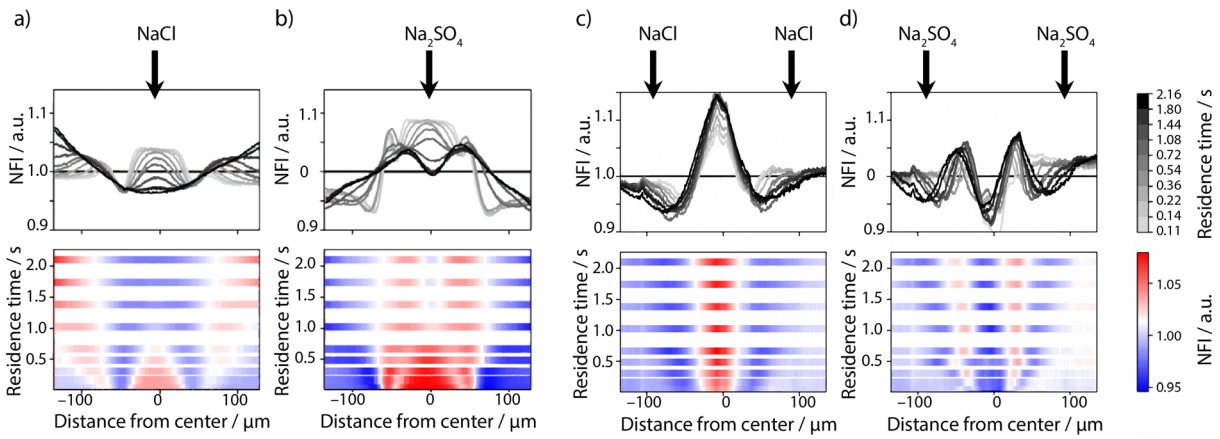

Fig. 3 The distribution of $[Ru(bpy)_3]Cl_2$ across the main channel of a three-inlet microfluidic device influenced by the addition of 1 M salt solutions *via* either the central inlet (shown by a single central arrow) of the two external inlets (indicated by two arrows). $[Ru(bpy)_3]Cl_2$ (50 μM in 50 mM MES buffer, pH 6) is pumped through the device *via* all three inlets and (a) 1 M NaCl is added *via* the central inlet, or (b) 1 M Na_2SO_4 is added *via* the central inlet or (c) 1 M NaCl is added *via* the external inlets or (d) 1 M Na_2SO_4 is added *via* the external inlets. Images were recorded 2 mm from the start of the channel. Residence times are determined by flow rate (20–1 μL min^{-1}). The data in both rows is the same but presented as normalised fluorescence intensity (NFI) or residence time.

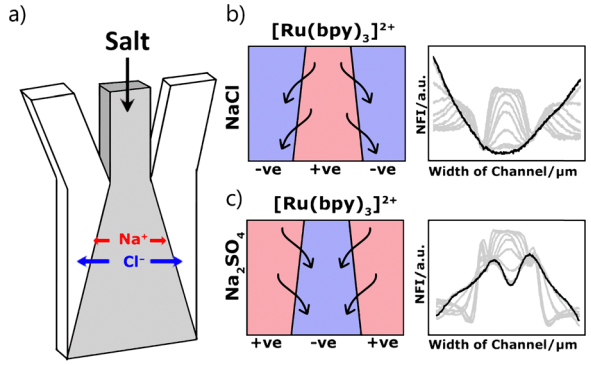

Fig. 4 (a) Schematic summary of the controlled displacement of the cationic dye $[Ru(bpy)_3]Cl_2$ following the addition of either sodium chloride or sodium sulfate to a three-inlet microfluidics device. (b) NaCl is added to the central inlet, a net positive charge is generated in the centre of the channel, and the dye migrates towards the walls of the channel; (c) Na_2SO_4 is added to the central channel, the dye is focused in the centre of the channel.

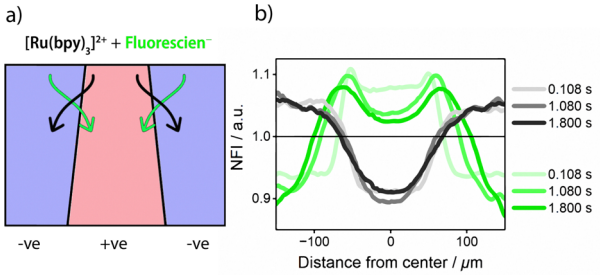

Fig. 5 (a) Controlling the separation of two dyes, $Ru(bpy)_3Cl_2$ (black) and fluorescein (green), in flow using passive electrophoresis in a three-inlet microfluidic device. A solution of $[Ru(bpy)_3]Cl_2$ and fluorescein (50 μM and 50 μM in 50 mM MES buffer, pH 6.5) is pumped through the device *via* all three inlets and 1 M NaCl is added *via* the central inlet. (b) Normalised fluorescence intensity (NFI) across the width of the channel for the two dyes, showing $Ru(bpy)_3Cl_2$ (excited by 458 nm) migrating to the edges of the channel and fluorescein (excited by 488 nm) being focussed into the centre. Images were recorded 2 mm from the start of the channel. Residence times are determined by flow rate (20–1.2 μL min^{-1}).

in the centre of the channel as the dye is concentrated into the centre. The focusing of the dye into the middle of the channel is more pronounced as twice as much salt is added when two inlets are used compared to the single central inlet. When sodium sulfate was added to the external inlets, propagating waves of the dye are observed on either side of the centre as the dye migrates towards the edges.

Increasing the salt concentration added to the central inlet (0.1, 0.25, 0.5 and 1.0 M) increased the displacement of the dye (see ESI,† S6). These experiments establish that simple salt gradients can control the migration of emissive ions over hundreds of micrometres, distances which enable controlled movement in microfluidic systems (Fig. 4). The three-inlet design allows both the focusing and dispersion of the emissive ion. The estimated potential based on the simulated ion concentrations is 8 mV, similar in magnitude to the membrane potential of erythrocytes (red blood cells) (see ESI,† S3).[26]

We then applied the system to separate species with different charges (Fig. 5). Solutions of $[Ru(bpy)_3]Cl_2$ and fluorescein were flowed through all three inlets and then sodium chloride was added to the central inlet, forming the liquid junction potential. The flow rates were varied from 20–1.2 μL min^{-1} and imaged using 458 nm and 488 nm excitation optimised using ZEN Black 2010 for the two dyes (see ESI,† S7). At pH 6.5, the two dyes are oppositely charged, the $[Ru(bpy)_3]Cl_2$ migrates to the edges of the channel, and the fluorescein is concentrated into the centre. The spectral properties of fluorescein did not significantly change in the presence of salt (see ESI,† S4).

The experiment was repeated with just fluorescein in the absence of $[Ru(bpy)_3]Cl_2$ (see ESI,† S8). While such movement in response to ionic gradients is obvious, microfluidic devices allow stable gradients to be generated under conditions suitable for the direct observation of molecular transport. Regulating the movement of photoredox catalysts like $Ru(bpy)_3Cl_2$ could allow spatial control of reactions. The generated liquid junction potentials could control the formation of concentration-dependent self-assemblies[27] and offer insight into how concentration gradients control the movement of species in biology.

This work was supported by the Australian Research Council (DP220101847). A. Sen acknowledges support by the Sloan Foundation. We acknowledge the Mark Wainwright Analytical Centre at UNSW Sydney for access to the NMR facility and the UNSW node of the NCRIS-enabled Australian National Fabrication Facility (ANFF) and Dr Jasper Fried for device fabrication. The imaging component of this study was carried out using instruments situated in, and maintained by, the Katharina Gaus Light Microscopy Facility (KGLMF) at UNSW.

Data availability

All data for this work is deposited on the ChemRxiv server, see L. L. Fillbrook, I. A. Middleton, H. Rashidnejad, A. Sapre, A. Sen, J. E. Beves, T. W. Schmidt. DOI: **10.26434/chemrxiv-2024-tvmn2-v3**.

Conflicts of interest

There are no conflicts to declare.

References

1 S. Sengupta, M. M. Spiering, K. K. Dey, W. Duan, D. Patra, P. J. Butler, R. D. Astumian, S. J. Benkovic and A. Sen, *ACS Nano*, 2014, **8**, 2410–2418.
2 M. Wanunu, W. Morrison, Y. Rabin, A. Y. Grosberg and A. Meller, *Nat. Nanotechnol.*, 2010, **5**, 160–165.
3 Y. A. Song, S. Hsu, A. L. Stevens and J. Han, *Anal. Chem.*, 2006, **78**, 3528–3536.
4 V. S. Doan, P. Saingam, T. Yan and S. Shin, *ACS Nano*, 2020, **14**, 14219–14227.
5 M. S. Munson, C. R. Cabrera and P. Yager, *Electrophoresis*, 2002, **23**, 2642–2652.
6 J. P. Ebel, J. L. Anderson and D. C. Prieve, *Langmuir*, 1988, **4**, 396–406.
7 A. Kar, T. Y. Chiang, I. Ortiz Rivera, A. Sen and D. Velegol, *ACS Nano*, 2015, **9**, 746–753.
8 J. Deseigne, C. Cottin-Bizonne, A. D. Stroock, L. Bocquet and C. Ybert, *Soft Matter*, 2014, **10**, 4795–4799.
9 S. Vrhovec Hartman, B. Bozic and J. Derganc, *New Biotechnol.*, 2018, **47**, 60–66.

10 B. Abécassis, C. Cottin-Bizonne, C. Ybert, A. Ajdari and L. Bocquet, *Nat. Mater.*, 2008, **7**, 785–789.
11 B. Abécassis, C. Cottin-Bizonne, C. Ybert, A. Ajdari and L. Bocquet, *New J. Phys.*, 2009, **11**.
12 R. Yadav, N. Sivoria and S. Maiti, *J. Phys. Chem. B*, 2024, **128**, 9573–9585.
13 V. S. Doan, I. Alshareedah, A. Singh, P. R. Banerjee and S. Shin, *Nat. Commun.*, 2024, **15**, 7686.
14 S. Sanchez, A. A. Solovev, S. M. Harazim and O. G. Schmidt, *J. Am. Chem. Soc.*, 2011, **133**, 701–703.
15 Y. Tu, F. Peng, X. Sui, Y. Men, P. B. White, J. C. M. van Hest and D. A. Wilson, *Nat. Chem.*, 2017, **9**, 480–486.
16 N. S. Mandal and A. Sen, *Langmuir*, 2021, **37**, 12263–12270.
17 K. T. Krist, A. Sen and W. G. Noid, *J. Chem. Phys.*, 2021, **155**, 164902.
18 N. S. Mandal, A. Sen and R. D. Astumian, *J. Am. Chem. Soc.*, 2023, **145**, 5730–5738.
19 N. S. Mandal, A. Sen and R. D. Astumian, *Chem*, 2024, **10**, 1147–1159.
20 J. M. Schurr, B. S. Fujimoto, L. Huynh and D. T. Chiu, *J. Phys. Chem. B*, 2013, **117**, 7626–7652.
21 J. Agudo-Canalejo, P. Illien and R. Golestanian, *Nano Lett.*, 2018, **18**, 2711–2717.
22 L. L. Fillbrook, J. P. Gunther, G. Majer, D. J. O'Leary, W. S. Price, H. Van Ryswyk, P. Fischer and J. E. Beves, *J. Am. Chem. Soc.*, 2021, **143**, 20884–20890.
23 F. Mohajerani, X. Zhao, A. Somasundar, D. Velegol and A. Sen, *Biochemistry*, 2018, **57**, 6256–6263.
24 D. R. Lide, *CRC Handbook of Chemistry and Physics: A Ready-reference Book of Chemical and Physical Data*, CRC-Press, 1995.
25 A. Juris, V. Balzani, F. Barigelletti, S. Campagna, P. Belser and A. von Zelewsky, *Coord. Chem. Rev.*, 1988, **84**, 85–277.
26 U. V. Lassen and O. Stenknud, *J. Physiol.*, 1968, **195**, 681–694.
27 W. Wang, Y.-X. Wang and H.-B. Yang, *Chem. Soc. Rev.*, 2016, **45**, 2656–2693.

